SpoVAF and FigP assemble into oligomeric ion channels that enhance spore germination

Yongqiang Gao,[1] Jeremy D. Amon,[1] Anna P. Brogan,[1] Lior Artzi,[1] Fernando H. Ramírez-Guadiana,[1] Joshua C. Cofsky,[2] Andrew C. Kruse,[2] and David Z. Rudner[1]

[1]Department of Microbiology, Harvard Medical School, Boston, Massachusetts 02115, USA; [2]Department of Biological Chemistry and Molecular Pharmacology, Harvard Medical School, Boston, Massachusetts 02115, USA

Bacterial spores can remain dormant for decades yet rapidly germinate and resume growth in response to nutrients. GerA family receptors that sense and respond to these signals have recently been shown to oligomerize into nutrient-gated ion channels. Ion release initiates exit from dormancy. Here, we report that a distinct ion channel, composed of SpoVAF (5AF) and its newly discovered partner protein, YqhR (FigP), amplifies the response. At high germinant concentrations, 5AF/FigP accelerate germination; at low concentrations, this complex becomes critical for exit from dormancy. 5AF is homologous to the channel-forming subunit of GerA family receptors and is predicted to oligomerize around a central pore. *5AF* mutations predicted to widen the channel cause constitutive germination during spore formation and membrane depolarization in vegetative cells. Narrow-channel mutants are impaired in germination. A screen for suppressors of a constitutively germinating 5AF mutant identified FigP as an essential cofactor of 5AF activity. We demonstrate that 5AF and FigP interact and colocalize with GerA family receptors in spores. Finally, we show that 5AF/FigP accelerate germination in *B. subtilis* spores that have nutrient receptors from another species. Our data support a model in which nutrient-triggered ion release by GerA family receptors activates 5AF/FigP ion release, amplifying the response to germinant signals.

[*Keywords*: germination; sporulation; dormancy; ion channel; GerA; signal transduction]

Supplemental material is available for this article.

Received November 13, 2023; revised version accepted January 4, 2024.

Bacteria in the orders *Bacillales* and *Clostridiales* are responsible for more than 1 million infections each year and account for huge monetary losses to the food industry (Mallozzi et al. 2010; Andre et al. 2017). These pathogens resist sterilization by differentiating into stress-resistant spores. Spores are metabolically inactive and can remain dormant for decades yet rapidly resume growth upon exposure to nutrients, causing food spoilage, food-borne illness, or life-threatening disease (Setlow 2014). The exit from dormancy, called germination, is a key target in combatting these pathogens. The germination program of most spore-forming bacteria involves a common series of chemical steps catalyzed by a small set of broadly conserved factors (Moir and Cooper 2015; Setlow et al. 2017). Germinant receptors embedded in the spore membrane monitor the environment for germination signals, typically amino acids, sugars, and/or nucleosides. These receptors are nutrient-gated ion channels, and detection of specific nutrients triggers the release of ions from the spore core (Gao et al. 2023). Evidence suggests that ion release activates the transport of large stores of dipicolinic acid (DPA) from the spore via the SpoVA (Spo5A or 5A) transport complex (Vepachedu and Setlow 2007; Gao et al. 2022, 2023). Released DPA in turn activates cell wall hydrolases that degrade the specialized peptidoglycan that encases the spore, allowing core rehydration, macromolecular synthesis, and resumption of growth (Setlow 2003; Moir 2006).

The prototypical germinant receptor in *Bacillus subtilis*, GerA, is composed of three broadly conserved subunits: GerAA, GerAB, and GerAC (Paredes-Sabja et al. 2011). GerAA and GerAB are polytopic membrane proteins, and GerAC is a lipoprotein (Moir and Cooper 2015). GerAA is predicted to oligomerize into a high-confidence pentamer or hexamer with a membrane channel at its oligomeric interface (Gao et al. 2023; Kilian and Bischofs 2023). Each GerAA protomer in the complex interacts with a GerAB subunit that is responsible for

Corresponding author: rudner@hms.harvard.edu
Article published online ahead of print. Article and publication date are online at http://www.genesdev.org/cgi/doi/10.1101/gad.351353.123.

L-alanine recognition (Artzi et al. 2021; Gao et al. 2023). Accordingly, a ring of ligand-binding subunits encircles the oligomeric channel. GerAC protomers are also predicted to oligomerize. Each GerAC protomer binds GerAB and GerAA and bridges neighboring GerAA protomers (Gao et al. 2023). In response to L-alanine, the nutrient-gated ion channel opens, releasing ions. Ion release in turn triggers expulsion of DPA from the spore core via a separate membrane complex encoded in the *spo5A* (or *5A*) locus (Fort and Errington 1985; Gao et al. 2022). The *B. subtilis 5A* locus consists of seven genes (*5AA*, *5AB*, *5AC*, *5AD*, *5AEb*, *5AEa*, and *5AF*), of which only three (*5AC*, *5AEb*, and *5AD*) are required for DPA export (Gao et al. 2022). The functions of the other genes in the *5A* operon are poorly understood. Interestingly, *5AF* encodes a homolog of the pore-forming GerAA protein (Errington 1993), suggesting that 5AF may also conduct ions or even play a role in germination-associated ion release. However, it is unclear how an additional ion channel would fit into a model that already contains nutrient-gated ion release by GerA family receptors.

Here, we report that the 5AF protein functions as an ion channel that amplifies nutrient-activated ion release in germinating spores. We show that spores lacking 5AF are impaired in ion release and subsequent steps in spore germination. In an unbiased screen for 5AF mutants that constitutively germinate, we identified amino acid substitutions in 5AF that are predicted to widen the membrane channel or stabilize it in an open conformation. Reciprocally, we engineered 5AF variants predicted to narrow the channel, which exhibited impaired ion release. Using one of the constitutive germination alleles, we screened for suppressors and identified YqhR (FigP) as an essential cofactor of 5AF. AlphaFold2-Multimer predicted that 5AF and FigP form a heterodimer that can oligomerize in a manner similar to the GerA complex. We demonstrate that 5AF and FigP interact, form oligomers in vivo, and colocalize with GerA family receptors in spores. We further show that expression of the channel-widening *5AF* allele during vegetative growth is toxic and causes loss of membrane potential, provided FigP is coexpressed. Finally, we show that 5AF/FigP amplify germination responses in *B. subtilis* spores even when germinant receptors or DPA transporters are replaced by homologs from *Bacillus megaterium*, *Clostridiodes difficile*, or *Bacillus cereus*. Collectively, our data support a model in which 5AF and FigP form an oligomeric membrane channel that releases ions in response to ion release by GerA family nutrient receptors, amplifying the germination response.

Results

5AF is predicted to oligomerize into a membrane channel and is required for ion release during germination

The last gene in the *B. subtilis 5A* locus, *5AF*, encodes a homolog of the channel-forming A subunits of GerA family receptors (Errington 1993; Perez-Valdespino et al. 2014). The AlphaFold-predicted structure of 5AF resembles the GerAA model, with a TM-align score of 0.69 and RMSD of 2.58 Å within the high-confidence regions of the model (Fig. 1A; Supplemental Fig. S1A). Furthermore, AlphaFold2-Multimer (Jumper et al. 2021; Evans et al. 2022) predicts that 5AF monomers assemble into a high-confidence pentamer surrounding a central channel, similar to the GerAA pentamer model (Fig. 1B; Supplemental Fig. S1B; Gao et al. 2023). AlphaFold2-Multimer also predicts that GerAA and, separately, 5AF can form high-confidence hexamers (Supplemental Fig. S1C; Kilian and Bischofs 2023). For clarity, we present the pentamer model throughout this article but are currently unable to experimentally distinguish between the two models.

The structural similarity of 5AF to GerAA motivated us to perform a more detailed analysis of 5AF. Although the *5AF* gene is in the *spo5A* locus, it is not required for DPA import into developing spores (Perez-Valdespino et al. 2014; Gao et al. 2022), and its role in germination is unclear. A deletion of *5AF* and the gene adjacent to it, *5AEa*, was previously reported to cause a delay in germination (Perez-Valdespino et al. 2014). Our analysis of in-frame deletions in *5AF* and separately in *5AEa* revealed that the loss of *5AF* was solely responsible for the delayed germination, as assessed by DPA release and optical density (Fig. 1C,D; Supplemental Fig. S2A–D). Furthermore, normal germination kinetics were restored to the Δ*5AF* mutant when *5AF* was expressed in *trans*.

To determine whether 5AF is involved in ion release, we exposed wild-type and Δ*5AF* spores to 10 mM L-alanine and analyzed the germination exudates using inductively coupled plasma mass spectrometry (ICP-MS). As shown in Figure 1E, Δ*5AF* spores were delayed in ion release, and expression of 5AF in *trans* restored wild-type release rates (Fig. 1E; Supplemental Fig. S3). These findings are consistent with the idea that 5AF oligomers function as ion channels and release ions in response nutrients, thereby accelerating exit from dormancy. Finally, we note that the correlation between delayed release of ions and delayed release of DPA provides additional support for the prevailing model that ion release is the activating signal for DPA export (Gao et al. 2023).

Spores lacking GerA are unable to germinate upon exposure to L-alanine (Moir and Cooper 2015; Setlow et al. 2017). However, Δ*gerA* spores germinate efficiently in the presence of asparagine, glucose, fructose, and K^+ ions (AGFK), which signal through the homologous GerB and GerK nutrient receptors. Similarly, Δ*gerA* spores germinate and form colonies on LB agar plates at efficiencies similar to that of wild type, but spores lacking GerA, GerB, and GerK are reduced in colony formation by ~500-fold (Supplemental Fig. S2E). To investigate whether 5AF responds to nutrients, we analyzed colony formation of Δ*5AF* spores and spores lacking *5AF* and all GerA family loci (Δ*ger5*): *gerA*, *gerB*, *gerK*, and two additional *ger* loci (*yndDEF* and *yfkQRT*) of unknown function (Paidhungat and Setlow 2000). Spores lacking 5AF formed colonies at efficiencies similar to that of wild type, and spores lacking 5AF and all GerA family receptors formed colonies at efficiencies similar to that of the Δ*ger5 gerA* family deletion strain (Supplemental Fig. S2E). The absence of any further reduction in colony formation suggests that 5AF does not

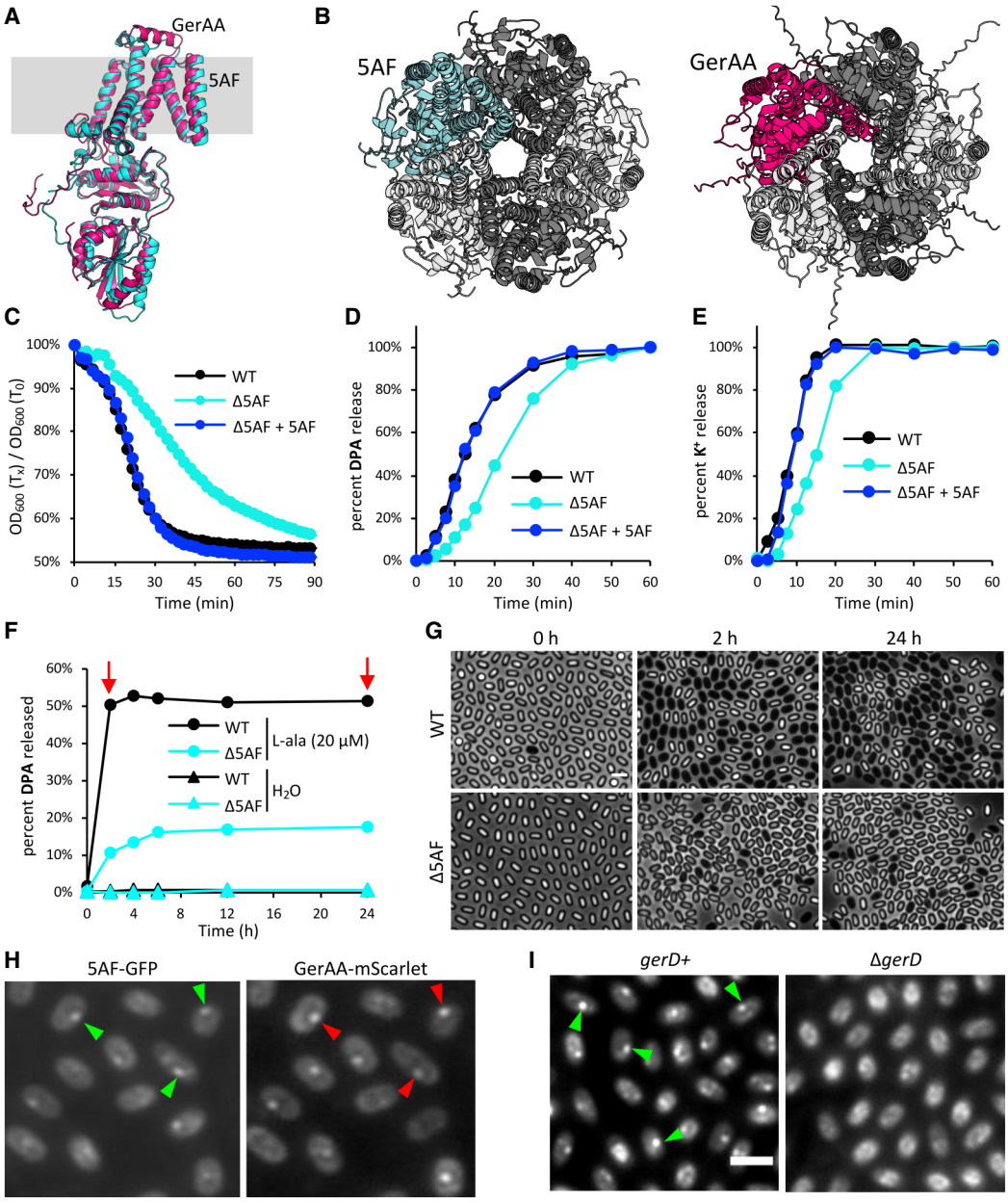

Figure 1. Spo5AF (5AF) is predicted to form an oligomeric membrane channel and is required for efficient ion release during germination. (*A*) Structural alignment by TM-align of the AlphaFold-predicted structures of GerAA (magenta) and 5AF (cyan). (*B*) AlphaFold-Multimer predictions of 5AF and GerAA pentamers viewed from outside the spore. Protomers are shown in dark and light gray and cyan (5AF) or magenta (GerAA). (*C*) Purified spores from wild type, Δ*5AF*, or Δ*5AF* complemented with *5AF* in *trans* were mixed with 10 mM L-alanine, and optical density was analyzed over 90 min. (*D*,*E*) The germination exudates from the same spores used in *C* were collected at the indicated times and analyzed for DPA (*D*) and K^+ (*E*). The percentage release at each time point, relative to the amount released by WT spores at 60 min, is shown. A complete analysis of ion release and biological replicates is shown in Supplemental Figure S3. (*F*) Purified WT and Δ*5AF* spores were incubated with and without 20 μM L-alanine without agitation for the indicated times in hours at 37°C. The percentage of DPA released relative to total is shown. Time points analyzed by phase-contrast microscopy are indicated (red arrows). (*G*) Representative phase-contrast images of WT and Δ*5AF* spores incubated with 20 μM L-alanine for the indicated times. (*H*) A functional 5AF-GFP fusion colocalizes with GerAA-mScarlet in dormant spores. Green and red arrowheads indicate colocalized germinosome foci. (*I*) GerD is required for 5AF-GFP foci in dormant spores. Scale bars, 2 μm.

directly respond to nutrients and instead is activated by the GerA family receptors.

Δ*5AF* spores exhibit a relatively modest delay in germination (Fig. 1C). We wondered whether our standard germination assays, in which we exposed spores to 1–10 mM L-alanine, were masking a more important role for this putative ion channel under conditions that more closely mimic those encountered in the environment.

To explore this possibility, we incubated wild-type and Δ*5AF* spores with low concentrations of nutrients (20 µM L-alanine) without agitation and monitored germination by phase-contrast microscopy and DPA release over 24 h. Approximately 60% of the total DPA in wild-type spores was released over the 24-h time course compared with ~10% in spores lacking 5AF (Fig. 1F). Phase-contrast microscopy revealed a similar reduction of phase-dark germinated spores in the Δ*5AF* mutant compared with wild type (Fig. 1G). These data argue that 5AF can significantly increase the number of spores that germinate over 24 h. Collectively, these findings support the idea that 5AF-dependent ion release amplifies GerA's response to L-alanine, which is even more critical under nutrient-poor conditions.

GerA family receptors have been shown to colocalize in foci called germinosomes in dormant spores (Griffiths et al. 2011). To investigate whether 5AF is also present in germinosomes, we generated a functional GFP fusion (Supplemental Fig. S4) and analyzed its localization. The 5AF-GFP fusion formed discrete foci that colocalized with GerAA-mScarlet (Fig. 1H). Importantly, the 5AF-GFP foci were lost in spores lacking GerD, a lipoprotein required for germinosome formation (Fig. 1I; Mongkolthanaruk et al. 2009; Griffiths et al. 2011). Altogether, we conclude that 5AF proteins are predicted to assemble into oligomeric ion channels and colocalize with GerA family nutrient-gated ion channels and are required for efficient ion release and exit from dormancy in response to nutrients.

An unbiased screen for 5AF *mutations that cause premature germination*

In a previous study, we identified constitutively active mutations in *gerAA* that caused developing spores to prematurely germinate. These alleles mapped to residues within or adjacent to the lumen of the predicted membrane channel of the GerAA oligomer, providing strong genetic support for the AlphaFold prediction (Gao et al. 2023). Accordingly, we performed an unbiased screen for constitutively active *5AF* alleles (Supplemental Fig. S5). Briefly, the *5AF* gene was PCR-mutagenized and transformed into a Δ*5AF* mutant, and the transformants were pooled and sporulated. We isolated prematurely germinated spores from denser dormant spores on a histodenz step gradient and inoculated them into rich medium that supports growth and efficient sporulation upon nutrient exhaustion. After a second round of enrichment, the prematurely germinated spores were plated onto sporulation agar plates, and the resulting colonies were sporulated for 96 h at 37°C. Spores from >200 individual colonies were analyzed by phase-contrast microscopy, and two mutants were identified that had high frequencies of premature germination: A360V and L367S (Fig. 2A; Supplemental Fig. S6A). Sporulated cultures of both mutants also displayed severe reductions in heat-resistant colony-forming units (CFUs) (Fig. 2A). The reduction in heat-resistant CFUs is particularly striking given that the Δ*5AF* mutant is not impaired in spore formation. Importantly, these mutant phenotypes did not require the GerA family receptors (Supplemental Fig. S6A). The L367S mutant mapped within the lumen of the channel model and is predicted to widen the pore. The A360V mutant mapped adjacent to the lumen and is predicted to stabilize an open conformation of the channel (Fig. 2B; Supplemental Fig. S7).

To further investigate the channel model, we substituted lumen-facing residues V371 and Q375 with leucines, which we predicted would narrow or occlude the channel (Fig. 2B). Both mutants formed phase-bright spores that were heat-resistant (Fig. 2C), similar to wild type and the Δ*5AF* mutant. However, when these spores were exposed to nutrients, they were delayed in ion release and all subsequent steps of germination (Fig. 2D; Supplemental Fig. S8). Similarly, when the mutant spores were exposed to low concentrations of L-alanine, they were impaired in exit from dormancy (Fig. 2E). Importantly, the mutant 5AF proteins were stable in dormant spores (Fig. 2F) and localized in germinosome foci (Fig. 2G), suggesting that the lumen-facing mutants assemble into complexes but are unable to amplify the GerA response to L-alanine. The discovery of germination-controlling mutations within the predicted membrane channel supports the AlphaFold model that 5AF oligomerizes into an ion channel.

Identification of YqhR (FigP) as a 5AF partner protein

GerAA resides in a complex with the nutrient-sensing subunit GerAB and the lipoprotein GerAC (Artzi et al. 2021; Amon et al. 2022; Gao et al. 2023). These three proteins depend on each other for stability in dormant spores and require each other for channel function in vegetatively growing cells (Cooper and Moir 2011; Mongkolthanaruk et al. 2011; Gao et al. 2023). We therefore wondered whether 5AF has one or more partner proteins. To search for potential interacting proteins, we screened for loss-of-function mutations that suppress the sporulation defect associated with the constitutive *5AF* allele A360V. We transposon-mutagenized cells harboring *5AF* (A360V*)* and then pooled and sporulated the transposon (Tn) library. The sporulated culture was subjected to 80° C for 20 min to kill vegetative cells that had failed to sporulate and spores that had prematurely germinated. The mixture was then plated on rich medium, allowing the heat-resistant spores to germinate and form colonies. The colonies were pooled and the Tn insertions were mapped by deep sequencing (Tn-seq). The screen identified five genes (*yqhR*, *ymfJ*, *ymfD*, *ytpA*, and *yktB*) that were enriched for Tn insertions compared with the input library (Fig. 3A; Supplemental Fig. S9A). The *yqhR*, *ymfJ*, and *ymfD* genes are expressed in the forespore under SigF or SigG control (Nicolas et al. 2012; Arrieta-Ortiz et al. 2015). *yqhR* encodes an uncharacterized membrane protein, *ymfJ* encodes a cytoplasmic protein with a DUF3243 domain, and *ymfD* encodes a putative transporter of the major facilitator superfamily. *ytpA* and *yktB* are expressed during vegetative growth and are not specifically induced during sporulation. *ytpA* encodes a

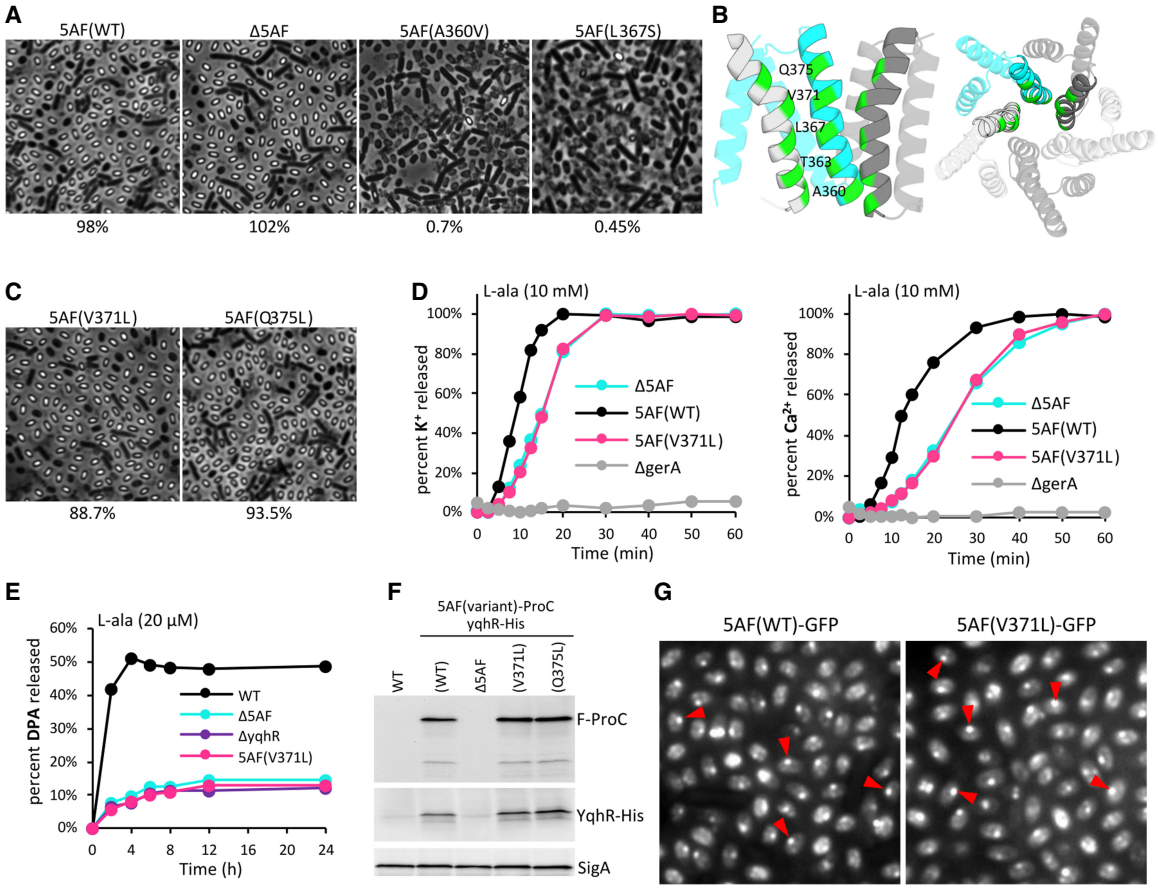

Figure 2. Characterization of 5AF mutants predicted to widen or narrow the membrane channel. (*A*) Representative phase-contrast images of sporulated cultures of strains with *5AF*(WT), Δ*5AF*, and the indicated constitutively active *5AF* alleles. Heat-resistant CFUs of each strain compared with wild type are shown *below* the images. (*B*) Side and top views of the three transmembrane helices that surround the membrane channel in the 5AF pentamer model. Residues identified in the screen and those that are predicted to line the channel are indicated. (*C*) Representative phase-contrast images of sporulated cultures of strains with *5AF* alleles predicted to narrow the channel. Percentages of heat-resistant CFUs are indicated *below* the images. (*D*) Purified spores from the indicated strains were mixed with 10 mM L-alanine, and the germination exudates were collected at the indicated times and analyzed for K^+ and Ca^{2+}. The percentage released at each time point, relative to the amount released by 5AF(WT) spores at 60 min, is shown. The channel-narrowing mutant *5AF*(V371L) phenocopies Δ*5FA*. Similar results were obtained for all steps in the germination pathway and with *5AF*(Q375L) and are shown in Supplemental Figure S8. (*E*) Purified spores of the indicated strains were germinated with 20 μM L-alanine without agitation, and the percentage of DPA released relative to total was monitored over time (in hours). Similar differences between WT and Δ5AF were observed at lower concentrations of L-alanine with agitation. (*F*) Immunoblots from lysates of the purified spores used in *D*. Functional ProteinC (ProC) fusions to 5AF(WT), 5AF(V371L), and 5AF(Q375L) are stable. σ^A (SigA) controlled for loading. YqhR-His is stable in the mutant spores. (*G*) Representative fluorescence images of functional GFP fusions to 5AF(WT) and 5AF(V371L) in dormant spores. Red arrowheads indicate germinosome foci.

putative phospholipase, and *yktB* encodes a cytoplasmic protein with a DUF1054 domain.

We tested in-frame deletions of all five genes and found that, to varying degrees, all five mutants suppressed the premature germination phenotype and the defect in heat-resistant CFUs of the *5AF*(V360A) mutant (Fig 3B; Supplemental Fig. S9B). Among the five mutants, the strongest suppressor was Δ*yqhR*, which largely restored wild-type percentages of phase-bright spores and heat-resistant CFUs to those of the constitutively active 5AF mutant. Analysis of spore germination of each mutant in a wild-type (*5AF*$^+$) background revealed that Δ*yqhR* phenocopied Δ*5AF* mutant spores, while Δ*ymfJ*, Δ*yktB*, and Δ*ymfD* had no impact on spore germination, and Δ*ytpA* had an intermediate phenotype (Fig. 3C; Supplemental Fig. S9C). Finally, only the Δ*5AF* Δ*yqhR* double mutant had a germination defect that resembled the single mutants (Fig. 3C; Supplemental Fig. S10). These data suggest that *5AF* and *yqhR* reside in the same genetic pathway and could function as partner proteins. We therefore focused on YqhR, which we have renamed FigP (for 5AF-interacting germination protein).

AlphaFold2-Multimer (Jumper et al. 2021; Evans et al. 2022) predicted a high-confidence interaction between 5AF and FigP, consistent with the idea that the two proteins form a complex (Fig. 3D; Supplemental Fig. S11).

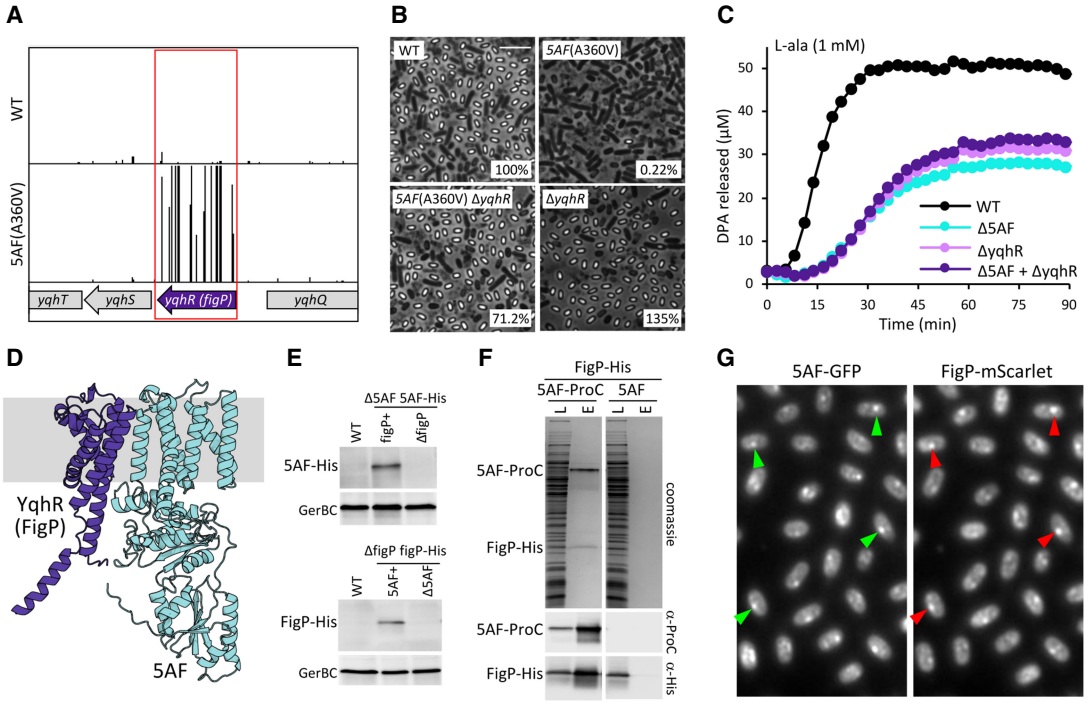

Figure 3. Identification and characterization of FigP, an essential 5AF cofactor. (*A*) A transposon sequencing (Tn-seq) screen for mutations that suppress the premature germination of *5AF*(A360V) identified *yqhR* (*figP*). Transposon insertion profiles from the *yqhR* region of the genome are shown. Tn libraries from wild type (WT) and 5AF(A360V) were sporulated, incubated for 20 min at 80°C, and plated on LB agar. The colonies were pooled and Tn sites were mapped by deep sequencing. Each line represents a Tn insertion site; the height reflects its abundance in the output library. The maximum number of reads was set at 10,000. Tn insertions in *yqhR* (*figP*) were overrepresented in 5AF(A360V) compared with WT. (*B*) Representative phase-contrast images of the indicated strains. Δ*yqhR* suppresses the premature germination phenotype of *5AF*(A360V). The percentages of heat-resistant spores compared with wild type are indicated in the *bottom right* corners of the images. (*C*) Purified spores from the indicated strains were mixed with 1 mM L-alanine, and DPA release was monitored over 90 min. (*D*) The AlphaFold-predicted complex of YqhR (FigP) is in purple and 5AF is in cyan. (*E*) 5AF and FigP depend on each other for stability in dormant spores. Representative immunoblots from lysates of dormant spores of the indicated strains. (*Top*) 5AF-His requires FigP for stability. (*Bottom*) FigP-His requires 5AF for stability. GerBC controlled for loading. (*F*) 5AF and FigP copurified from detergent-solubilized membrane preparations derived from exponentially growing *B. subtilis* cells engineered to express FigP-His and 5AF-ProC. (*Top*) Coomassie-stained gel of load (L) and elution (E) from anti-ProC resin. (*Bottom*) Immunoblots from the same purification probing for 5AF-ProC and FigP-His. (*G*) 5AF-GFP and FigP-mScarlet colocalize in dormant spores. Representative fluorescence images of spores with 5AF-GFP and FigP-mScarlet. Colocalizing germinosome foci are indicated by green and red arrowheads.

In addition, we found that the two proteins depend on each other for stability in dormant spores (Fig. 3E). The instability of 5AF in the absence of FigP provides an explanation for how *figP* mutants suppress the premature germination of *5AF*(A360V). Further support for the idea that the two proteins interact comes from copurification of FigP-His with 5AF-ProteinC (5AF-ProC) from detergent-solubilized membrane preparations of *B. subtilis* cells expressing the two functional fusion proteins (Fig. 3F; Supplemental Fig. S4). Finally, a functional FigP-mScarlet fusion colocalized with 5AF-GFP in germinosome foci in dormant spores (Fig. 3G). Altogether, we conclude that FigP resides in a complex with 5AF and likely functions with 5AF to amplify the germination response.

5AF/FigP assemble into an oligomeric complex

In the AlphaFold models, FigP binds to a site on 5AF that is analogous to GerAB's binding site on GerAA, though FigP is not homologous to GerAB (Supplemental Fig. S12). AlphaFold-Multimer predicted that the GerAA/GerAB/GerAC heterotrimer can oligomerize without clashes between protomers (Gao et al. 2023). Similarly, AlphaFold2-Multimer predicted that the 5AF/FigP dimer can assemble into a high-confidence oligomer of heterodimers without clashes between subunits (Fig. 4A; Supplemental Fig. S11). These data are consistent with the idea that FigP functions in complex with 5AF.

Evidence that the GerA complex acts as an ion channel comes from experiments in which vegetative expression of constitutively active alleles of *gerAA* were toxic due to membrane depolarization, provided *gerAB* and *gerAC* were coexpressed (Gao et al. 2023). To investigate whether 5AF and FigP can similarly form a toxic membrane channel, we expressed wild-type *5AF* and the channel-widening *5AF* allele, *5AF*(L367S), under an IPTG-regulated promoter in the presence and absence of FigP. 5AF (L367S) was toxic only if FigP was coexpressed (Fig. 4B).

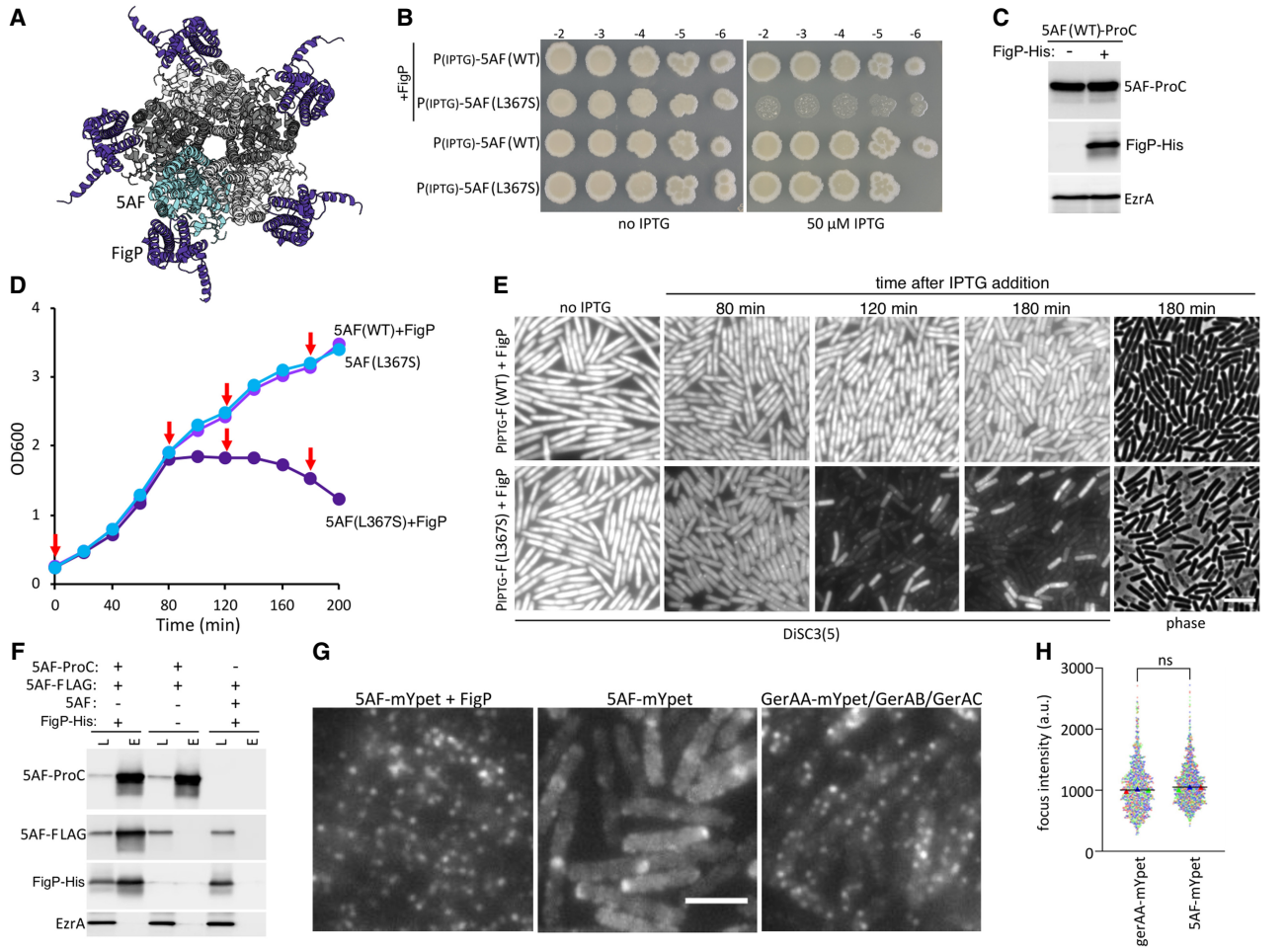

Figure 4. 5AF and FigP reside in an oligomeric complex that has properties of ion channels. (*A*) AlphaFold2-Multimer prediction of the 5AF/FigP oligomer. 5AF protomers are shown in cyan and light/dark gray. FigP protomers are in purple. (*B*) Expression of the channel-widening 5AF(L367S) is toxic to *B. subtilis*, provided FigP is coexpressed. Representative spot dilutions of the indicated strains on LB agar in the absence and presence of 50 µM IPTG. (*C*) Representative immunoblots from the indicated exponentially growing *B. subtilis* strain. 5AF-ProC is stable in the presence and absence of FigP during vegetive growth, unlike dormant spores. EzrA controlled for loading. (*D*) Representative growth curves of the indicated strains after the addition of IPTG at time 0. Both the *5AF*(WT) and *5AF*(L367S) alleles are under the control of the IPTG-regulated promoter Phyperspank, and FigP was expressed constitutively. (*E*) Representative fluorescence and phase-contrast images of the cells in *D* at the indicated times after IPTG addition using the potentiometric dye $DiSC_3(5)$. Membrane potential drops over time in cells expressing 5AF(L367S) and FigP. Cell lysis, as assayed by phase contrast, only occurs at later time points. A more complete time course, including staining with propidium iodide, is shown in Supplemental Figure S13. (*F*) Differentially tagged 5AF proteins copurify, provided FigP is present. Immunoblots of the load (L) and elution (E) of the indicated strains expressing 5AF-ProC, 5AF-FLAG, and FigP-His. Detergent-solubilized membrane proteins from exponentially growing *B. subtilis* cells were subjected to immunoaffinity purification using anti-ProC resin. EzrA served as a negative control. (*G*) Representative fluorescence images of exponentially growing *B. subtilis* cells expressing 5AF-mYpet in the presence and absence of FigP. Cells expressing GerAA-mYpet with GerAB and GerAC are shown for comparison. Discrete foci of 5AF-mYpet require FigP. The foci are of intensities similar to that of GerAA-mYpet in the presence of GerAB and GerAC. Scale bars, 5 µm. (*H*) Quantification of fluorescence intensities of GerAA-mYpet and 5AF-mYpet foci in the presence of their partner proteins. Three biological replicates (>500 cells for each) were quantified and are plotted in different colors. No significant (ns) difference in focus intensity was observed.

Importantly, unlike the situation in dormant spores, 5AF was stable in the absence of FigP in vegetatively growing cells (Fig. 4C). Thus, the lack of toxicity when 5AF (L367S) was expressed on its own argues that FigP is required for 5AF to assemble into a stable oligomer and/or form a functional channel.

To investigate whether 5AF(L367S)/FigP toxicity was due to loss of membrane potential, we induced the expression of 5AF(WT)/FigP, 5AF(L367S), or 5AF(L367S)/FigP in rich medium and analyzed membrane potential over time using the potentiometric dye $DiSC_3(5)$. Eighty minutes after expression of 5AF(L367S)/FigP, the culture stopped increasing in optical density, whereas at later time points the optical density began to drop, consistent with lysis (Fig. 4D). In contrast, cells expressing 5AF(L367S) without FigP or 5AF(WT) with FigP continued to grow for the full

time course. Importantly, membrane potential of cells expressing 5AF(L367S)/FigP gradually decreased over time, and the cells eventually lysed (Fig. 4E; Supplemental Fig. S13). Analysis of membrane permeability using propidium iodide indicated that the loss of membrane potential preceded the loss of membrane integrity (Supplemental Fig. S13). Cells expressing 5AF(WT)/FigP or 5AF(L367S) without FigP maintained membrane potential and membrane integrity throughout the induction time course (Fig. 4E; Supplemental Fig. S13). These experiments support the model that the 5AF/FigP complex forms an ion channel.

5AF oligomerizes in vivo

To directly test whether 5AF oligomerizes in vivo, we first tested whether FLAG-tagged 5AF could be copurified with 5AF-ProC from vegetatively growing *B. subtilis*. As shown in Figure 4F, anti-ProC resin efficiently copurified 5AF-ProC and 5AF-FLAG from cells that coexpressed FigP. In the absence of FigP, 5AF-FLAG was not copurified with 5AF-ProC (Fig. 4F). These data indicate that at least two 5AF protomers reside in a complex that depends on FigP. In a second experiment, we analyzed 5AF-mYpet localization in exponentially growing *B. subtilis*. We previously showed that expression of GerAA-mYpet in vegetative cells forms fluorescent foci when GerAB and GerAC are coexpressed (Fig. 4G; Gao et al. 2023). Importantly, increasing GerAA-mYpet expression in the presence of GerAB and GerAC increased the number of foci but not their fluorescence intensity, suggesting that each focus represents a discrete oligomeric complex (Supplemental Fig. S14). Here, we coexpressed 5AF-mYpet in the presence and absence of FigP. 5AF-mYpet formed discrete foci, provided FigP was present, and the number of foci but not their intensity increased with increasing 5AF-mYpet expression (Fig. 4G; Supplemental Figs. S14, S15). Importantly, both qualitatively and quantitatively, the 5AF-mYpet/FigP foci resembled GerAA-mYpet/GerAB/GerAC foci (Fig. 4H), arguing that 5AF/FigP form discrete oligomeric complexes that are similar in stoichiometry to GerA complexes. Finally, to investigate whether 5AF forms an oligomeric complex in spores, we coexpressed wild-type 5AF and the channel-blocking mutant 5AF(V371L) in sporulating cells. The resulting spores displayed a delay in germination that was similar to Δ5AF and 5AF(V371L) mutant spores (Supplemental Fig. S16). These data indicate that *5AF*(V371L) is a strong dominant-negative allele, consistent with this channel-blocking mutant poisoning wild-type 5AF protomers in an oligomeric complex. Collectively, these experiments provide strong support for the model that 5AF/FigP assembles into an oligomeric complex around a central channel.

5AF/FigP enhances germination triggered by a nonnative GerA family receptor and DPA release by nonnative DPA transporters

Our data support a model in which the 5AF/FigP complex is activated by ion release from GerA family receptors, and the release of ions by both complexes promotes DPA export by the 5A transporter. In this model, both the activation of 5AF/FigP by GerA receptors and the activation of the DPA transport complex do not involve protein–protein interactions and are instead mediated by chemical or physical changes in the spore. To further test this model, we took advantage of our previous findings that the GerA family receptor GerUV from *Bacillus megaterium* is functional in *B. subtilis* spores (Christie and Lowe 2007; Gao et al. 2023). Similarly, we previously showed that the DPA transport complexes from *Clostridiodes difficile* and *Bacillus cereus* can replace the native *B. subtilis 5A* locus. Importantly neither the *C. difficile 5A* operon nor the *B. cereus 5A-2* locus encodes a 5AF homolog (Berendsen et al. 2016; Donnelly et al. 2016; Baloh and Sorg 2021). We analyzed spore germination rates in strains complemented by these nonnative loci in the presence and absence of 5AF. As shown in Figure 5, spores harboring *gerUV*(*Bm*) and lacking all GerA family receptors released DPA faster in response to glucose, leucine, proline, and K^+ (GLPK) in the presence of 5AF than in its absence. Similarly, spores harboring 5A (*Cd*) or 5A-2(*Bc*) released DPA faster when 5AF was present than in its absence (Fig. 5B; Supplemental Fig. S17). These data are consistent with a model in which initial nutrient-stimulated ion release by GerA family channels triggers ion release by the 5AF/FigP complex. Faster ion release more efficiently activates DPA expulsion from the 5A transport complex (Fig. 6).

Discussion

Spores can remain dormant for decades yet constantly survey their environment for nutrients and the opportunity to germinate and resume growth. Here, we have shown that the 5AF/FigP complex functions to amplify the germination response when nutrients are detected. When spores are exposed to high concentrations of germinants, this complex plays a relatively minor role, accelerating germination by 10–20 min. However, in the presence of low concentrations of nutrients, 5AF/FigP can significantly increase the number of spores that germinate over 24 h. Our data suggest that 5AF/FigP enhances nutrient detection by releasing ions in response to ion release by GerA family receptors (Fig. 6). Faster release of ions by these related ion channels more efficiently triggers DPA export by the 5A complex, leading to activation of cortex lytic enzymes. The 5AF/FigP signal amplifier is not essential for germination and is not as broadly conserved as GerA family receptors or the core components of the DPA transport complex encoded in the *5A* operon. However, FigP homologs are present in most *Bacilli* and co-occur with the poorly characterized 5AA and 5AB proteins encoded in the *5A* locus (Supplemental Fig. S18). Our data indicate that 5AF/FigP can accelerate germination of spores harboring the *B. megaterium* GerUV receptor and, separately, spores harboring *C. difficile* or *B. cereus* 5AC/5AD/5AEb. We therefore suspect that 5AF/FigP complexes both sense ion release and use ion release to activate DPA export in all spore formers that encode them.

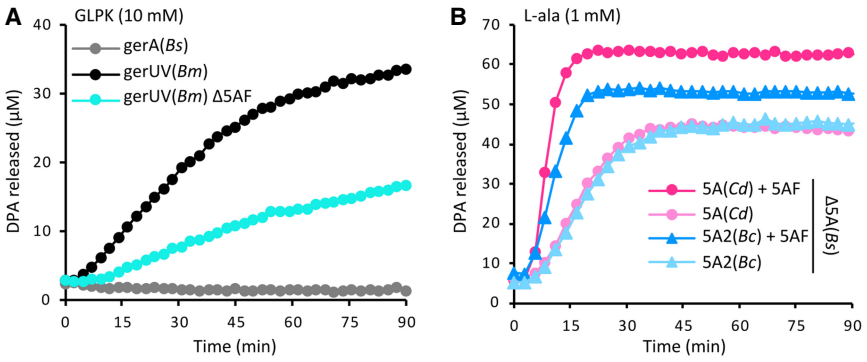

Figure 5. 5AF enhances germination of *B. subtilis* spores with a nonnative germination receptor or nonnative DPA transport complexes. (*A*) Purified *B. subtilis* spores lacking all five endogenous germinant receptor loci and harboring the *gerUV*(*Bm*) or *gerA*(*Bs*) locus were incubated with 10 mM glucose, leucine, proline, and K^+ (GLPK), and DPA release was monitored over 90 min. Cells lacking 5AF germinated more slowly. (*B*) Purified spores lacking the native *5A* operon and harboring an ectopic copy of the *5A* locus from *C. difficile* (*Cd*) or the *5A2* locus from *B. cereus* (*Bc*) were incubated with 1 mM L-alanine, and DPA release was monitored over 90 min. Neither *5A2*(*Bc*) nor *5A*(*Cd*) encodes a 5AF homolog. *B. subtilis* 5AF was expressed in *trans* in the indicated strains.

The mechanism by which 5AF/FigP complexes are activated by GerA-type receptors remains to be elucidated. One possible model relates to the colocalization of these complexes in spores. Previous studies have shown that Δ*gerD* spores that lack clustered nutrient receptors germinate more slowly (Li et al. 2014). This finding suggests that receptor clustering could amplify nutrient detection by conformational spreading within the oligomeric array, increasing ligand affinity, as has been proposed for chemotaxis receptors (Rao et al. 2004; Sourjik and Berg 2004; Briegel et al. 2014). In the context of this model, 5AF/FigP could be activated by conformational spreading within the germinosome. However, we found that Δ*gerD* mutant spores are further impaired in germination if they also lack 5AF (Supplemental Fig. S19), suggesting that 5AF can be activated by GerA receptors without clustering with them. We favor an alternative model in which the 5AF/FigP oligomer functions as a voltage-gated ion channel (Bezanilla 2008, 2018) that is activated when an initial GerA-catalyzed ion release changes the membrane voltage.

It is noteworthy that the AlphaFold-predicted FigP model is structurally homologous to INSIG1 (insulin-induced gene 1), which is involved in cholesterol homeostasis in mammals (Yang et al. 2002). Mammalian INSIG1 has been shown to bind 5-hydroxycholesterol and function with sterol response element binding protein (SREBP) cleavage-activating protein (SCAP) to control SREBP-mediated transcription (Hua et al. 1996). The predicted FigP structure is most similar to the mycobacterial INSIG1 homolog MvINS from *Mycobacterium vanbaalenii* (Supplemental Fig. S20), which has not been characterized in vivo (Ren et al. 2015). Intriguingly, a crystal structure of MvINS was determined with diacylglycerol bound in its conserved membrane pocket, raising the possibility that FigP also binds a lipid (Supplemental Fig. S20). Amino acid substitutions in either of two tyrosines in FigP that are predicted to face the conserved pocket partially impaired FigP function, slowing the rate of germination (Supplemental Fig. S20). Both mutant proteins were stable in spores and stabilized 5AF (Supplemental Fig. S20). These results are consistent with the idea that FigP binds a lipid and argue that FigP has a function beyond simply stabilizing the 5AF oligomer. It is possible that lipid binding by FigP could function as the trigger for channel opening. If this model is correct, the activating lipids would have to be kept away from the 5AF/FigP oligomers during spore formation and dormancy and would only access the complexes after the onset of germination, perhaps due to changes in membrane fluidity (Cowan et al. 2003; Flores et al. 2023). Alternatively, we speculate that changes in membrane voltage due to ion release by GerA family receptors are transduced through the lipid–FigP interaction. The role of lipid–FigP binding and how ion release activates 5AF/FigP and in turn triggers DPA release by the 5A complex remain important and outstanding questions for future investigation.

Materials and methods

General methods

All strains used in this study were derived from *Bacillus subtilis 168* (Zeigler et al. 2008). Sporulation was induced by nutrient exhaustion in complete Difco sporulation medium (DSM) for 30 h at 37°C (Schaeffer et al. 1965), and sporulation efficiency was determined by comparing heat-resistant (for 20 min at 80°C) colony-forming units (CFUs) of mutants with wild-type *B. subtilis 168*. All in-frame deletion mutants were derived from *Bacillus* knockout collection (BKE) (Koo et al. 2017) or constructed by direct transformation of isothermal assembly products into competent *B. subtilis*. Antibiotic cassettes were excised using a temperature-sensitive plasmid that constitutively expresses Cre recombinase (Meeske et al. 2015). Site-directed mutants were generated using a modified QuickChange protocol. Strains, plasmids, and oligonucleotide primers used in this study are in Supplemental Tables S1–S3. Experiments presented in the text and supplemental figures were from one of at least three biological replicates, with the exception of Figures 2F, 3E, and 4C and Supplemental Figures S16A, S18E, and S19, which were from two biological replicates.

Spore purification

To generate spores used for immunoblot analysis or to determine the total DPA content, cells were grown in

DSM for 3 h at 37°C to an OD_{600} of 0.2–0.3 and then spread on DSM agar plates, followed by incubation for 96 h at 37°C. Spores were scraped from the plates, washed three times with ddH_2O, and then resuspended in PBS supplemented with 1.5 mg/mL lysozyme. After incubation for 1 h at 37°C, SDS was added to the final concentration of 2% (w/v), and the spores were incubated for 30 min at 37°C and then washed five times with ddH_2O.

To generate purified phase-bright spores for germination assays and microscopy analysis, spores were scraped from DSM agar plates as described above. The spores were washed three times with ddH_2O and then resuspended in 350 µL of 20% histodenz (Sigma-Aldrich). The suspension was layered on top of 1 mL of 50% histodenz in a microfuge tube, and the step gradient was centrifuged at 15,000 rpm for 30 min. The pellet fraction containing the phase-bright spores was collected and washed five times with ddH_2O.

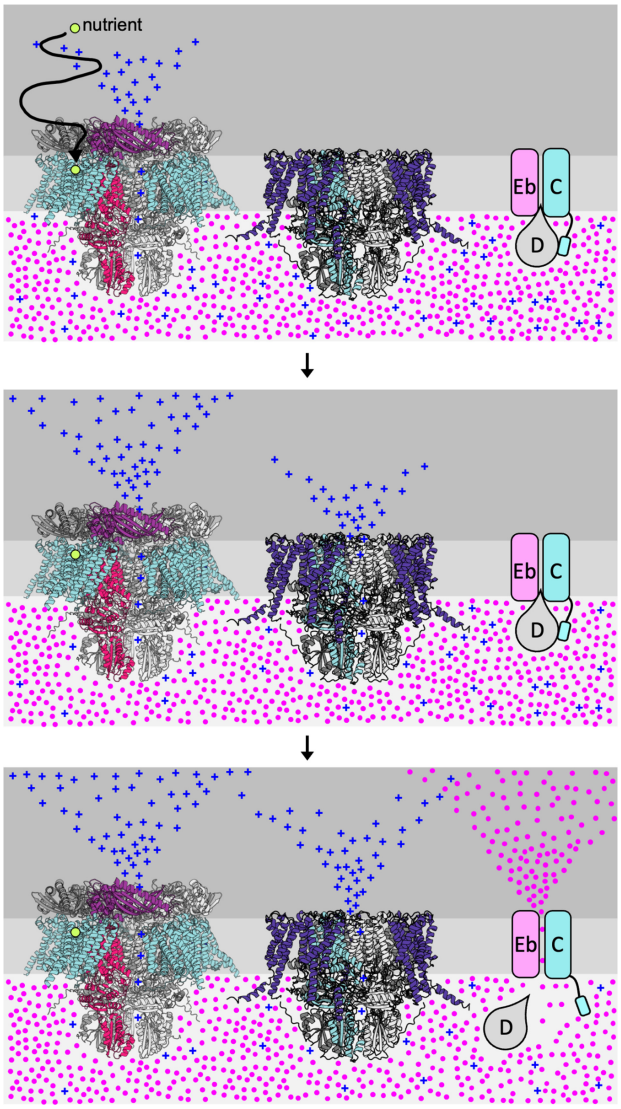

Figure 6. 5AF/FigP amplifies the germination response by releasing ions. Schematic model of the germination pathway in *B. subtilis*. (*Top* panel) Nutrients are detected by the B subunits (cyan) of GerA family receptors. Ligand binding causes channel opening of the A subunits and ion release. Monovalent cations (blue pluses) are shown, but the identity of the cation (or anion) that triggers downstream steps is currently unknown. (*Middle* panel) Ion release by GerA family receptors induces channel opening of 5AF in the 5AF/FigP complex, resulting in ion release and amplification of the response. (*Bottom* panel) A drop in core ion concentration and/or a change in membrane potential causes "unplugging" of 5D (D) from the 5C/5Eb (C/Eb) channel and release of DPA. DPA activates the cortex-degrading enzyme CwlJ (not shown). A second cortex-degrading enzyme, SleB (also not shown), is activated by an unknown mechanism. Together, these enzymes degrade the cortex, enabling full hydration of the core and the onset of macromolecular synthesis.

DPA quantification

Purified spores were normalized to an OD_{600} of 1 in 1 mL of ddH_2O, and the spore suspension was incubated for 30 min at 100°C to release DPA. After centrifugation at 15,000 rpm for 5 min, 300 µL of the supernatant was collected and mixed with 300 µL of 100 µM $TbCl_3$. Next, 150 µL of the mixture was transferred to a black, flat-bottom, 96-well plate, and the fluorescence signal was measured at 545 nm with excitation at 272 nm using an Infinite M Plex plate reader (Tecan). Each sample was analyzed in technical triplicate and compared with a standard curve generated using purified DPA (Sigma-Aldrich).

DPA release assay

Histodenz-purified phase-bright spores were normalized to an OD_{600} of 1 in 25 mM HEPES (pH 7.4) and heat-activated for 30 min at 70°C, followed by incubation for 15 min on ice. Seventy-five microliters of the spore suspension was transferred to a black, flat-bottom, 96-well plate, and an equal volume of 25 mM HEPES (pH 7.4; buffer), 2 or 20 mM L-alanine, 20 mM AGFK (20 mM L-asparagine, D-glucose, fructose, and KCl), and 20 mM GLPK (20 mM D-glucose, L-leucine, L-proline, and KBr) resuspended in 25 mM HEPES (pH 7.4) was added to the spores. All nutrients and buffer contained 100 µM $TbCl_3$, resulting in a final concentration of 50 µM. The fluorescence was monitored at 545 nm with excitation at 272 nm every 2 min for 2 h in an Infinite M Plex plate reader (Tecan). The 96-well plate was maintained at 30°C and agitated between measurements. All spore samples and conditions were tested in technical triplicate and compared with a standard curve.

Reduction in optical density (OD_{600}) assay

Histodenz-purified phase-bright spores were normalized to an OD_{600} of 1.2 in 25 mM HEPES (pH 7.4) and heat-activated for 30 min at 70°C, followed by incubation for 15 min on ice. One-hundred microliters of spore suspension was then transferred to a clear, flat-bottom, 96-well plate. An equal volume of nutrients or buffer as described above was added to the spore suspension for a final OD_{600} of 0.6. The OD_{600} was monitored every 2 min for 4 h using an infinite M Plex plate reader (Tecan). The plate was

maintained at 37°C with agitation between measurements. All samples were analyzed in technical triplicate.

DPA release assay with low concentration of L-alanine

Histodenz-purified phase-bright spores were normalized to an OD_{600} of 1 in ddH_2O or 20 µM L-alanine and then incubated at 37°C without agitation. Five-hundred microliters of the spore suspension was collected at the indicated times, followed by centrifugation at 15,000 rpm for 5 min. Next, 450 µL of supernatant was mixed with an equal volume of 100 µM $TbCl_3$ and analyzed for DPA as described above. The spore pellets were analyzed by phase-contrast microscopy.

Cation release assay using inductively coupled plasma mass spectrometry (ICP-MS)

Histodenz-purified phase-bright spores were normalized to an OD_{600} of 5 in 20 mL of ddH_2O and heat-activated for 30 min at 70°C, followed by incubation for 15 min on ice. One milliliter of the spore suspension was mixed with 1 mL of ddH_2O and boiled for 30 min to release all DPA and ions from the spore core. The supernatant was collected and stored on ice. The remaining 19 mL of spore suspension was prewarmed for 20 min at 37°C, followed by the addition of an equal volume of 20 mM L-alanine. The mixture was vortexed and incubated at 37°C. At the indicated time points, 2 mL of the spore suspension was collected, and the germination exudate (the supernatant) was collected by centrifugation at 15,000 rpm for 30 sec. Next, 1.8 mL of the supernatant was transferred to a fresh microfuge tube (avoiding the spore pellet) and stored on ice until all samples were collected. In all cases, the spore suspension was collected ~30 sec prior to the indicated time point.

Upon completion of the time course, the germination exudates were separately passed through 0.2-µm syringe filters to remove all particulates. Next, 150 µL of the filtrate was used for DPA quantification by mixing with an equal volume of 100 µM $TbCl_3$ and then analyzed as described above. The remaining 1.6 mL of filtered germination exudate was mixed with 400 µL of 10% nitric acid. The concentrations of K^+, Mg^{2+}, and Ca^{2+} in these samples were quantified using an Agilent 7900 inductively coupled plasma mass spectrometer in the Center for Environmental Health Sciences Bioanalytical Core Facility at Massachusetts Institute of Technology. The instrument was operated in helium mode. All samples were analyzed in biological triplicate. A standard curve for each cation was generated prior to analyzing the germination exudates for each ICP-MS experiment using ultrapure stocks of KCl, $MgCl_2$, and $CaCl_2$ (Avantor). The concentration of ions present prior to L-alanine addition was subtracted from the concentrations at all time points after addition. The data were plotted as a percentage of ion released based on the concentration released by WT spores at 60 min after L-alanine addition.

Screen for constitutively active 5AF mutants

The *spoVAF* (*5AF*) gene was PCR-amplified with primers oYG417 and oYG418 using an error-prone Pfu polymerase (Biles and Connolly 2004), and pYG156 harboring the *5AF* gene and a *kan* cassette were used as templates. The mutagenized PCR product was cloned into pCB179 [*yhdG*::*spec* (*amp*)], cut with SpeI and XhoI by isothermal assembly, and transformed into *E. coli* DH5α. Approximately 130,000 transformants were pooled and stored −80°C. Plasmids from 20 individual transformants were isolated and subjected to Sanger sequencing using oYG380 and oYG17. Approximately 30 kb was sequenced and 37 mutations were identified for an average of ~1.2 mutations per kilobase (1.85 mutations per gene). The plasmid library was isolated using a minipreparation kit (Zymo Research) and transformed into the host strain bYG516 (Δ*sleB::lox72* Δ*spoVAF::lox72 yhdG::erm*), and ~80,000 transformants were pooled and stored in 15% glycerol stock at −80°C.

To screen for constitutively active *5AF* mutants, the pooled *B. subtilis* library was grown in liquid DSM for 30 h at 37°C. The sporulated cultures were washed three times with ddH_2O and layered on a histodenz step gradient. The supernatant "step" fraction containing vegetatively growing cells and germinated phase-gray spores lacking DPA was isolated and resuspended in PBS supplemented with 1.5 mg/mL lysozyme. After incubation for 1 h at 37°C, SDS was added to a final concentration of 2% (w/v), and cells were incubated for 30 min at 37°C and then washed five times with ddH_2O. The phase-gray spores were further purified on a histodenz step gradient. The purified spores were incubated with freshly prepared Ca^{2+}-DPA (equal volumes of 120 mM $CaCl_2$ and 120 mM DPA in Tris-HCl at pH 8.0). The mixture was rolled for 2 h at 22°C to activate the cortex-lytic enzyme CwlJ. The mixture was then serially diluted and spread on LB agar followed by incubation overnight at 37°C. Approximately 16,000 colonies were pooled for another round of enrichment as described above.

After a second round of enrichment, >200 individual colonies were picked and streaked on sporulation (DSM) agar and incubated for 96 h at 37°C, followed by analysis by phase-contrast microscopy to screen for phase-gray spores, indicative of premature germination. Genomic DNAs (gDNAs) from mutants with phase-gray spores were then isolated and transformed into the parental strain (bYG516) for validation. The gDNAs were also used to transform bYG25 (Δ*spoVAF::lox72 yhdG::erm*), and the resulting strains were tested for premature germination and the production of phase-dark and lysed spores. The *5AF* gene was PCR-amplified from the gDNAs of positive hits using oCB63 and oYG381, and the product was analyzed by Sanger sequencing using oYG380 and oYG17.

Microscopy

Samples were concentrated by centrifugation at 8000 rpm and immobilized on 1.5% agarose pads. Phase-contrast microscopy and fluorescence microcopy were performed

using a Nikon TE2000 inverted microscope equipped with a plan apo 100×/1.4 oil Ph3 DM objective lens and a CoolSNAP HQ2 monochrome CCD camera (Photometrics). For all sporulation cultures and purified phase-bright spores, the exposure time for both GFP and mScarlet fusions was 800 msec. For exponentially growing cells, the exposure time for both 5AF-GFP and 5AF-mYpet was 500 msec. Image analysis and processing were performed using Fiji or MetaMorph software (version 7.7, Molecular Devices).

Quantification of fluorescence intensities of 5AF-mYpet and GerAA-mYpet foci

To quantify the fluorescent foci of 5AF-mYpet and GerAA-mYpet in the presence of FigP or GerAB and GerAC, respectively, the strains (bYG1664 and bYG1179) were grown in LB medium supplemented with 1 mM IPTG for 3–4 h, and fluorescent images were captured as described above and analyzed using an ImageJ plug-in in MicrobeJ (Ducret et al. 2016). Briefly, all single cells in the phase-contrast channel were detected based on the following parameters: cell area: >1.1 μm^2, cell length: >1 µm, cell width: between 0.5 and 2 µm, and cell angularity: <0.5 rad. All 5AF-mYpet or GerAA-mYpet foci were detected in each cell by setting the fluorescent tolerance value in "Maxima" to 200. Both the focus intensity (mean value) and the average fluorescence intensity (mean value) per cell were quantified. In a subset of cells, the foci were too crowded to accurately detect and quantify individual foci. To enable the analysis, cells with average fluorescence intensity >800 were removed, and only foci in cells with an average fluorescence intensity <800 were analyzed. The data were plotted in GraphPad Prism.

Analysis of membrane potential and membrane permeability

Strains were grown in 30 mL of LB medium at 37°C. When the OD_{600} reached 0.2–0.3, IPTG was added to a final concentration of 50 µM. One milliliter of culture was collected at the indicated time points, 200 µL of culture was stained with the potentiometric fluorescent dye 3,3′-dipropylthiadicarbocyanine iodide [$DiSC_3(5)$; 1 µM final; Invitrogen], and 600 µL of culture was mixed with propidium iodide (PI; 0.5 µM final; Sigma-Aldrich). The cells were then immobilized on 1.5% agarose pads and analyzed by fluorescence microscope using the RFP/mCherry filter set on a Nikon TE2000 inverted microscope equipped with a plan apo 100×/1.4 oil Ph3 DM objective lens and a CoolSNAP HQ2 monochrome CCD camera (Photometrics). The exposure time for both $DiSC_3(5)$ and PI was 200 msec. Image analysis and processing were performed using Fiji or GraphPad Prism [version 9.4.1(458)].

Coexpression and purification of 5AF and FigP from exponentially growing B. subtilis

B. subtilis strains (bYG1144, bYG1201, bYG1184, bYG1280, and bYG1265) harboring IPTG- and xylose-regulated alleles of *5AF* and *FigP* were precultured in LB at 37°C to an OD_{600} of 0.6 and then diluted into 1 L of LB medium supplemented with 1 mM IPTG and 33 mM xylose at an OD_{600} of 0.01. Cells were grown with aeration for ~4 h at 37°C and harvested at an OD_{600} of ~1 by centrifugation at 8000 rpm for 15 min. The pellets were washed twice with 1× SMM (0.5 M sucrose, 20 mM maleic acid, 20 mM $MgCl_2$, adjusted to pH 6.5) and resuspended in in 40 mL of 1× SMM containing 0.5 mg/mL lysozyme. The cells were gently agitated for ~60 min at room temperature until >95% of the cells had converted into protoplasts as determined by phase-contrast microscopy.

The protoplasts were pelleted and lysed in 45 mL of cold hypotonic buffer (50 mM HEPES at pH 7.6, 150 mM NaCl, 20 mM $MgCl_2$, 1 mM DTT) supplemented with 5 U/mL of benzonase (Sigma-Aldrich) and 1× complete protease inhibitor (Roche). The lysate was subjected to ultracentrifugation at 35,000 rpm for 60 min at 4°C. The membrane pellet was resuspended in 50 mL of homogenization buffer (20 mM HEPES at pH 7.6, 150 mM NaCl, 20% glycerol) supplemented with 1% n-dodecyl-β-D-maltopyranoside (DDM) using a glass homogenizer. The solubilized suspension was rotated for 2 h at 4°C, followed by ultracentrifugation at 35,000 rpm for 60 min at 4°C. The supernatant containing detergent-solubilized membrane proteins was supplemented with 2 mM $CaCl_2$ and loaded onto a Bio-Rad column containing 1.5 mL of homemade anti-ProteinC antibody resin. The anti-ProteinC antibody resin was made by incubating anti-ProteinC monoclonal antibodies with CNBr-activated Sepharose 4B (Cytiva). The resin was washed with 25 column volumes (CV) of wash buffer (20 mM HEPES at pH 7.6, 150 mM NaCl, 20% glycerol, 2 mM $CaCl_2$, 0.1% DDM), and proteins were eluted with 5 CVs of elution buffer (20 mM HEPES at pH 7.6, 150 mM NaCl, 10% glycerol, 0.1% DDM, 5 mM EDTA at pH 8.0, 0.4 mg/mL ProC peptide [EDQVDPRLIDGK, Genscript]). The eluted proteins were resolved by SDS-PAGE on 17.5% acrylamide gels, followed by Coomassie blue (InstantBlue) staining or analysis by immunoblot as described below.

Transposon sequencing (Tn-seq) screen

Transposon insertion sequencing (Tn-seq) was performed on two independently generated libraries as described previously (Meeske et al. 2015). Briefly, the transposon plasmid pFR38 harboring the *Himar1* C9 transposase *erm* and the *spec* cassette flanked by inverted terminal repeats, one of which contained an MmeI site, was transformed into WT and bYG584 [*Δ5AF::lox72 ycgO::P_{VA}-spoVAF* (A360V); referred to here as 5AF*]. Erythromycin/lincomycin-resistant transformants were grown in LB medium supplemented with 100 µg/mL spectinomycin overnight at 20°C. The cultures were aliquoted and frozen in 15% glycerol. An aliquot was thawed and plated on LB agar plates supplemented with 100 µg/mL spectinomycin and incubated overnight at 42°C. Approximately 1 million colonies for each Tn library were scraped, pooled, aliquoted, and frozen in 15% glycerol.

An aliquot of the library was thawed, washed in sporulation (DSM complete) medium, and diluted into 50 mL of DSM at an OD_{600} of 0.05. The cultures were incubated at 37°C with agitation. Samples were harvested at an early stage of starvation (input) and 36 h later (T36). The T36 samples were incubated for 20 min at 80°C to kill nonsporulated cells and prematurely germinated spores and then plated on LB agar. Heat-resistant spores that could germinate and form colonies overnight at 37°C were then pooled (~750,000 colonies). Genomic DNA was isolated from the input and output samples and digested with MmeI, followed by adaptor ligation. The transposon–chromosome junctions were amplified in 18 PCR cycles, and the PCR products were gel-purified and sequenced on the Illumina HiSeq platform using TruSeq reagents (Tufts University Core Facility [TUCF]). The reads were mapped to the *B. subtilis 168* genome (NCBI NC_000964.3) using Bowtie 1.0.0. The genes in which reads were statistically overrepresented or underrepresented in the 5AF*(output) library compared with the WT (output) library were visualized using Artemis (version 18.1.0; Sanger Institute).

Lysates and immunoblot analysis

Spore lysates were generated from spores purified on a histodenz step gradient or by lysozyme-SDS as described above. Spores were resuspended in 500 µL of cold PBS supplemented with 1 mM phenylmethylsulfonyl fluoride (PMSF) and transferred to 2-mL tubes containing lysis matrix B (MP Biomedicals). After incubation for 15 min on ice, the spores were lysed using FastPrep (MP Biomedicals) at 6.5 m/sec for 60 sec. An equal volume of 2× sample buffer (4% SDS, 250 mM Tris at pH 6.8, 20% glycerol, 10 mM EDTA, Bromophenol blue) containing 10% β-mercaptoethanol was immediately added to the tubes and vortexed. After centrifugation at 15,000 rpm for 5 min, the supernatant was collected and total protein was quantified by a noninterfering protein assay (G-Biosciences). The normalized protein samples were resolved by SDS-PAGE on 17.5% polyacrylamide gels and transferred to an Immobilon-P membrane (Millipore).

Vegetative cell lysates were generated from *B. subtilis* cultures grown in LB medium. Briefly, cells were harvested at an OD_{600} of 0.5–0.8 and normalized to an OD_{600} of 0.5. One milliliter of normalized culture was centrifuged, and the cell pellet was resuspended in 50 µL of lysis buffer (20 mM Tris at pH 7.5, 10 mM EDTA, 1 mg/mL lysozyme [Sigma-Aldrich], 1 mM PMSF, 10 µg/mL DNase I [NEB], 100 µg/mL RNase A [NEB], 10 µg/mL leupeptin [Fisher Scientific], 10 µg/mL pepstatin [Fisher Scientific]) and incubated for 10 min at 37°C, followed by addition of an equal volume of 2× sample buffer containing 10% β-mercaptoethanol. The lysates were resolved by SDS-PAGE on 17.5% acrylamide gels and transferred to an Immobilon-P membrane (Millipore).

The PVDF membranes were blocked in 5% nonfat milk dissolved in 1× PBS with 0.5% Tween-20 (PBST) and then probed with anti-His (1:4000; GenScript), anti-ProC (1:1000) (Gao et al. 2023), anti-FLAG (1:5000; Sigma-Aldrich), anti-SigA (1:10,000) (Fujita and Sadaie 1998), anti-EzrA (1:10,000) (Levin et al. 1999), anti-GerBC (1:5000) (Stewart et al. 2012), or anti-SpoVAD (1:10,000) (Vepachedu and Setlow 2005) antibodies diluted in 3% BSA dissolved in PBST. After washing in PBST, the primary antibodies were detected with goat antirabbit or antimouse antibodies coupled to horseradish peroxidase (Bio-Rad) and detected and visualized by Western Lightning ECL reagent (PerkinElmer).

Structural modeling using AlphaFold-Multimer

All predicted structures were generated using AlphaFold-Multimer-v2 or AlphaFold-Multimer-v3 and ColabFold (Jumper et al. 2021; Evans et al. 2022), run locally on the Harvard Medical School O2 computing cluster or the Lambda Cloud computing server. General parameters were as follows: Multiple sequence alignments (MSA) were built using mmseqs2. Sequences from the same operon were paired in the MSA, and both paired and unpaired sequences were used to generate models. Five models were generated in each run, and each model was relaxed using AMBER and ranked by pTM score. Homologous templates found in the PDB were used. For the SpoVAF pentamer and the SpoVAF-FigP pentamer of dimers, the maximum number of model recycling was set to 12, and the top-ranked models were used throughout the text.

Data availability

All data are available here and in the Supplementary Material.

Competing interest statement

The authors declare no competing interests.

Acknowledgments

We thank all members of the Bernhardt-Rudner supergroup for helpful advice, discussions, and encouragement; Andrea Vettiger and the Harvard Medical School Microscopy Resources on the North Quad (MicRoN) Core for advice on microscopy and analysis; and the Center for Environmental Health Sciences Bioanalytical Core Facility at Massachusetts Institute of Technology for access to their inductively coupled plasma–mass spectrometer. Portions of this research were conducted on the O2 High-Performance Computing Cluster, supported by the Research Computing Group, at Harvard Medical School. Support for this work comes from National Institutes of Health grants GM145299, AI171308 (to D.Z.R.), and AI164647 (to D.Z.R. and A.C.K.). J.D.A. was funded by National Institutes of Health grant F32GM130003. A.P.B. was funded in part by the National Science Foundation (DGE1745303). L.A. was a Simons Foundation fellow of the Life Sciences Research Foundation. J.C.C. is a fellow of the Helen Hay Whitney Foundation.

Author contributions: Y.G. conceived and designed the study, acquired materials, analyzed and interpreted the

data, wrote the draft of the manuscript, gave final approval for the study, and is accountable for the results. J.D.A. conceived the study, analyzed and interpreted the data, and edited the manuscript. A.P.B. and J.C.C. analyzed and interpreted the data and edited the manuscript. L.A. conceived the study. F.H.R.-G. acquired materials and edited the manuscript. A.C.K. conceived and supervised the study, interpreted the data, and edited and gave final approval of the manuscript. D.Z.R. conceived, designed, and supervised the study; designed, analyzed, and interpreted the data; wrote the draft of the manuscript; gave final approval of the manuscript; and is accountable for the results.

References

Amon JD, Artzi L, Rudner DZ. 2022. Genetic evidence for signal transduction within the *Bacillus subtilis* GerA germinant receptor. *J Bacteriol* **204:** e0047021. doi:10.1128/jb.00470-21

André S, Vallaeys T, Planchon S. 2017. Spore-forming bacteria responsible for food spoilage. *Res Microbiol* **168:** 379–387. doi:10.1016/j.resmic.2016.10.003

Arrieta-Ortiz ML, Hafemeister C, Bate AR, Chu T, Greenfield A, Shuster B, Barry SN, Gallitto M, Liu B, Kacmarczyk T, et al. 2015. An experimentally supported model of the *Bacillus subtilis* global transcriptional regulatory network. *Mol Syst Biol* **11:** 839. doi:10.15252/msb.20156236

Artzi L, Alon A, Brock KP, Green AG, Tam A, Ramírez-Guadiana FH, Marks D, Kruse A, Rudner DZ. 2021. Dormant spores sense amino acids through the B subunits of their germination receptors. *Nat Commun* **12:** 6842. doi:10.1038/s41467-021-27235-2

Baloh M, Sorg JA. 2021. Clostridioides difficile SpoVAD and SpoVAE interact and are required for dipicolinic acid uptake into spores. *J Bacteriol* **203:** e0039421. doi:10.1128/JB.00394-21

Berendsen EM, Boekhorst J, Kuipers OP, Wells-Bennik MH. 2016. A mobile genetic element profoundly increases heat resistance of bacterial spores. *ISME J* **10:** 2633–2642. doi:10.1038/ismej.2016.59

Bezanilla F. 2008. How membrane proteins sense voltage. *Nat Rev Mol Cell Biol* **9:** 323–332. doi:10.1038/nrm2376

Bezanilla F. 2018. Gating currents. *J Gen Physiol* **150:** 911–932. doi:10.1085/jgp.201812090

Biles BD, Connolly BA. 2004. Low-fidelity *Pyrococcus furiosus* DNA polymerase mutants useful in error-prone PCR. *Nucleic Acids Res* **32:** e176. doi:10.1093/nar/gnh174

Briegel A, Wong ML, Hodges HL, Oikonomou CM, Piasta KN, Harris MJ, Fowler DJ, Thompson LK, Falke JJ, Kiessling LL, et al. 2014. New insights into bacterial chemoreceptor array structure and assembly from electron cryotomography. *Biochemistry* **53:** 1575–1585. doi:10.1021/bi5000614

Christie G, Lowe CR. 2007. Role of chromosomal and plasmid-borne receptor homologues in the response of *Bacillus megaterium* QM B1551 spores to germinants. *J Bacteriol* **189:** 4375–4383. doi:10.1128/JB.00110-07

Cooper GR, Moir A. 2011. Amino acid residues in the GerAB protein important in the function and assembly of the alanine spore germination receptor of *Bacillus subtilis 168*. *J Bacteriol* **193:** 2261–2267. doi:10.1128/JB.01397-10

Cowan AE, Koppel DE, Setlow B, Setlow P. 2003. A soluble protein is immobile in dormant spores of *Bacillus subtilis* but is mobile in germinated spores: implications for spore dormancy. *Proc Natl Acad Sci* **100:** 4209–4214. doi:10.1073/pnas.0636762100

Donnelly ML, Fimlaid KA, Shen A. 2016. Characterization of clostridium difficile spores lacking either SpoVAC or dipicolinic acid synthetase. *J Bacteriol* **198:** 1694–1707. doi:10.1128/JB.00986-15

Ducret A, Quardokus EM, Brun YV. 2016. Microbej, a tool for high throughput bacterial cell detection and quantitative analysis. *Nat Microbiol* **1:** 16077. doi:10.1038/nmicrobiol.2016.77

Errington J. 1993. *Bacillus subtilis* sporulation: regulation of gene expression and control of morphogenesis. *Microbiol Rev* **57:** 1–33. doi:10.1128/mr.57.1.1-33.1993

Evans R, O'Neill M, Pritzel A, Antropova N, Senior A, Green T, Žídek A, Bates R, Blackwell S, Yim J, et al. 2022. Protein complex prediction with AlphaFold-Multimer. bioRxiv. doi:10.1101/2021.10.04.463034

Flores MJ, Duricy K, Choudhary S, Laue M, Popham DL. 2023. A family of spore lipoproteins stabilizes the germination apparatus by altering inner spore membrane fluidity in *Bacillus subtilis* spores. *J Bacteriol* **205:** e0014223. doi:10.1128/jb.00142-23

Fort P, Errington J. 1985. Nucleotide sequence and complementation analysis of a polycistronic sporulation operon, spoVA, in *Bacillus subtilis*. *J Gen Microbiol* **131:** 1091–1105.

Fujita M, Sadaie Y. 1998. Promoter selectivity of the *Bacillus subtilis* RNA polymerase σ^A and σ^H holoenzymes. *J Biochem* **124:** 89–97. doi:10.1093/oxfordjournals.jbchem.a022102

Gao Y, Barajas-Ornelas RDC, Amon JD, Ramírez-Guadiana FH, Alon A, Brock KP, Marks DS, Kruse AC, Rudner DZ. 2022. The SpoVA membrane complex is required for dipicolinic acid import during sporulation and export during germination. *Genes Dev* **36:** 634–646. doi:10.1101/gad.349488.122

Gao Y, Amon JD, Artzi L, Ramírez-Guadiana FH, Brock KP, Cofsky JC, Marks DS, Kruse AC, Rudner DZ. 2023. Bacterial spore germination receptors are nutrient-gated ion channels. *Science* **380:** 387–391. doi:10.1126/science.adg9829

Griffiths KK, Zhang J, Cowan AE, Yu J, Setlow P. 2011. Germination proteins in the inner membrane of dormant *Bacillus subtilis* spores colocalize in a discrete cluster. *Mol Microbiol* **81:** 1061–1077. doi:10.1111/j.1365-2958.2011.07753.x

Hua X, Nohturfft A, Goldstein JL, Brown MS. 1996. Sterol resistance in CHO cells traced to point mutation in SREBP cleavage-activating protein. *Cell* **87:** 415–426. doi:10.1016/S0092-8674(00)81362-8

Jumper J, Evans R, Pritzel A, Green T, Figurnov M, Ronneberger O, Tunyasuvunakool K, Bates R, Žídek A, Potapenko A, et al. 2021. Highly accurate protein structure prediction with AlphaFold. *Nature* **596:** 583–589. doi:10.1038/s41586-021-03819-2

Kilian M, Bischofs IB. 2023. Co-evolution at protein–protein interfaces guides inference of stoichiometry of oligomeric protein complexes by de novo structure prediction. *Mol Microbiol* **120:** 763–782. doi:10.1111/mmi.15169

Koo BM, Kritikos G, Farelli JD, Todor H, Tong K, Kimsey H, Wapinski I, Galardini M, Cabal A, Peters JM, et al. 2017. Construction and analysis of two genome-scale deletion libraries for *Bacillus subtilis*. *Cell Syst* **4:** 291–305.e7. doi:10.1016/j.cels.2016.12.013

Levin PA, Kurtser IG, Grossman AD. 1999. Identification and characterization of a negative regulator of FtsZ ring formation in *Bacillus subtilis*. *Proc Natl Acad SciE* **96:** 9642–9647. doi:10.1073/pnas.96.17.9642

Li Y, Jin K, Ghosh S, Devarakonda P, Carlson K, Davis A, Stewart KA, Cammett E, Pelczar Rossi P, Setlow B, et al. 2014.

Structural and functional analysis of the GerD spore germination protein of *Bacillus* species. *J Mol Biol* **426:** 1995–2008. doi:10.1016/j.jmb.2014.02.004

Mallozzi M, Viswanathan VK, Vedantam G. 2010. Spore-forming *Bacilli* and *Clostridia* in human disease. *Future Microbiol* **5:** 1109–1123. doi:10.2217/fmb.10.60

Meeske AJ, Sham LT, Kimsey H, Koo BM, Gross CA, Bernhardt TG, Rudner DZ. 2015. MurJ and a novel lipid II flippase are required for cell wall biogenesis in *Bacillus subtilis*. *Proc Natl Acad Sci* **112:** 6437–6442. doi:10.1073/pnas.1504967112

Moir A. 2006. How do spores germinate? *J Appl Microbiol* **101:** 526–530. doi:10.1111/j.1365-2672.2006.02885.x

Moir A, Cooper G. 2015. Spore germination. *Microbiol Spectr* **3**. doi:10.1128/microbiolspec.TBS-0014-2012

Mongkolthanaruk W, Robinson C, Moir A. 2009. Localization of the GerD spore germination protein in the Bacillus subtilis spore. *Microbiology (Reading)* **155:** 1146–1151. doi:10.1099/mic.0.023853-0

Mongkolthanaruk W, Cooper GR, Mawer JS, Allan RN, Moir A. 2011. Effect of amino acid substitutions in the GerAA protein on the function of the alanine-responsive germinant receptor of *Bacillus subtilis* spores. *J Bacteriol* **193:** 2268–2275. doi:10.1128/JB.01398-10

Nicolas P, Mäder U, Dervyn E, Rochat T, Leduc A, Pigeonneau N, Bidnenko E, Marchadier E, Hoebeke M, Aymerich S, et al. 2012. Condition-dependent transcriptome reveals high-level regulatory architecture in *Bacillus subtilis*. *Science* **335:** 1103–1106. doi:10.1126/science.1206848

Paidhungat M, Setlow P. 2000. Role of ger proteins in nutrient and nonnutrient triggering of spore germination in *Bacillus subtilis*. *J Bacteriol* **182:** 2513–2519. doi:10.1128/JB.182.9.2513-2519.2000

Paredes-Sabja D, Setlow P, Sarker MR. 2011. Germination of spores of *Bacillales* and *Clostridiales* species: mechanisms and proteins involved. *Trends Microbiol* **19:** 85–94. doi:10.1016/j.tim.2010.10.004

Perez-Valdespino A, Li Y, Setlow B, Ghosh S, Pan D, Korza G, Feeherry FE, Doona CJ, Li YQ, Hao B, et al. 2014. Function of the SpoVAEa and SpoVAF proteins of *Bacillus subtilis* spores. *J Bacteriol* **196:** 2077–2088. doi:10.1128/JB.01546-14

Rao CV, Frenklach M, Arkin AP. 2004. An allosteric model for transmembrane signaling in bacterial chemotaxis. *J Mol Biol* **343:** 291–303. doi:10.1016/j.jmb.2004.08.046

Ren R, Zhou X, He Y, Ke M, Wu J, Liu X, Yan C, Wu Y, Gong X, Lei X, et al. 2015. Crystal structure of a mycobacterial Insig homolog provides insight into how these sensors monitor sterol levels. *Science* **349:** 187–191. doi:10.1126/science.aab1091

Schaeffer P, Millet J, Aubert JP. 1965. Catabolic repression of bacterial sporulation. *Proc Natl Acad Sci* **54:** 704–711. doi:10.1073/pnas.54.3.704

Setlow P. 2003. Spore germination. *Curr Opin Microbiol* **6:** 550–556. doi:10.1016/j.mib.2003.10.001

Setlow P. 2014. Spore resistance properties. *Microbiol Spectr* **2**. doi:10.1128/microbiolspec.TBS-0003-2012

Setlow P, Wang S, Li YQ. 2017. Germination of spores of the orders *Bacillales* and *Clostridiales*. *Annu Rev Microbiol* **71:** 459–477. doi:10.1146/annurev-micro-090816-093558

Sourjik V, Berg HC. 2004. Functional interactions between receptors in bacterial chemotaxis. *Nature* **428:** 437–441. doi:10.1038/nature02406

Stewart KA, Yi X, Ghosh S, Setlow P. 2012. Germination protein levels and rates of germination of spores of Bacillus subtilis with overexpressed or deleted genes encoding germination proteins. *J Bacteriol* **194:** 3156–3164. doi:10.1128/JB.00405-12

Vepachedu VR, Setlow P. 2005. Localization of SpoVAD to the inner membrane of spores of *Bacillus subtilis*. *J Bacteriol* **187:** 5677–5682. doi:10.1128/JB.187.16.5677-5682.2005

Vepachedu VR, Setlow P. 2007. Role of SpoVA proteins in release of dipicolinic acid during germination of *Bacillus subtilis* spores triggered by dodecylamine or lysozyme. *J Bacteriol* **189:** 1565–1572. doi:10.1128/JB.01613-06

Yang T, Espenshade PJ, Wright ME, Yabe D, Gong Y, Aebersold R, Goldstein JL, Brown MS. 2002. Crucial step in cholesterol homeostasis: sterols promote binding of SCAP to INSIG-1, a membrane protein that facilitates retention of SREBPs in ER. *Cell* **110:** 489–500. doi:10.1016/S0092-8674(02)00872-3

Zeigler DR, Prágai Z, Rodriguez S, Chevreux B, Muffler A, Albert T, Bai R, Wyss M, Perkins JB. 2008. The origins of 168, W23, and other *Bacillus subtilis* legacy strains. *J Bacteriol* **190:** 6983–6995. doi:10.1128/JB.00722-08